Earth Syst. Dynam. Discuss., https://doi.org/10.5194/esd-2017-54
Manuscript under review for journal Earth Syst. Dynam.
Discussion started: 6 June 2017

Earth System Dynamics Discussions

Influence of atmospheric internal variability on the long-term Siberian water cycle during the past two centuries

Kazuhiro Oshima[1], Koto Ogata[2,3], Hotaek Park[1], Yoshihiro Tachibana[2]

[1] Institute of Arctic Climate and Environment Research, Japan Agency for Marine-Earth Science and Technology, Yokosuka, Japan
[2] Weather and Climate Dynamics Division, Mie University, Tsu, Japan
[3] Aerological Observatory, Japan Meteorological Agency, Tsukuba, Japan

Correspondence to: Kazuhiro Oshima (kazuhiroo@jamstec.go.jp)

Abstract. River discharges from Siberia are a large source of freshwater into the Arctic Ocean, although the cause of the long-term variation in discharge is still unclear. The observed river discharges of the Lena in the east and the Ob in the west indicated different relationships in each of the epochs during the past seven decades. The correlations between the two river discharges were negative during the 1980s to mid-1990s, positive during the mid-1950s to 1960s, and became weak after the mid-1990s. Long-term records of tree-ring-reconstructed discharges during the past two centuries have also shown differences in the correlations in each epoch. However, it is noteworthy that the correlations obtained from the reconstructions tend to be negative. Such negative correlations have also been obtained from precipitations over the Lena and Ob in observation, and in simulations with an atmospheric general circulation model (AGCM) and multi-coupled models conducted for the Fourth Assessment Report of the IPCC. The AGCM control simulation further demonstrated that an east–west seesaw pattern of summertime atmospheric large-scale circulation frequently emerges over Siberia as an atmospheric internal variability, resulting in the negative correlation between the Lena and Ob. Consequently, the summertime atmospheric internal variability of east–west seesaw pattern over Siberia is a key factor influencing the long-term variation in precipitation and river discharge, i.e., the water cycle in this region.

1 Introduction

The river discharge (*R*) from the pan-Arctic terrestrial area supplies freshwater, nutrients, and organic matter to the Arctic Ocean. The three great Siberian rivers, the Lena, Yenisei and Ob account for about 60% of the total *R* into the Arctic Ocean and have an important role in the freshwater budget and climate system in the Arctic (e.g., Aagaard and Carmack, 1989, 1994). Numerous studies have investigated the interannual variation and linear trend of the Siberian *R* (e.g., Berezovskaya, et al., 2004; Ye et al., 2004; McClelland et al., 2004, 2006; Rawlins et al., 2006; MacDonald et al., 2007; Shiklomanov and Lammers, 2009), however they have mainly analyzed the *R* dataset from a hydrological perspective. Several other studies have been conducted to determine the linkages among atmospheric circulation, moisture transport, precipitation (*P*), precipitation minus evapotranspiration (*P*-*E*), and the *R* for Siberian rivers using atmospheric reanalysis

Earth Syst. Dynam. Discuss., https://doi.org/10.5194/esd-2017-54
Manuscript under review for journal Earth Syst. Dynam.
Discussion started: 6 June 2017

Earth System Dynamics Discussions Open Access EGU

combined with the *R* dataset (Fukutomi et al., 2003; Serreze et al., 2003; Zhang et al., 2012; Oshima et al., 2015). To understand such linkages, it is necessary to improve our knowledge of the terrestrial and atmospheric water cycle in the region.

Theoretically, *P*-*E* over a basin, which is the net input of water from the atmosphere to the land surface, corresponds to *R* at the river mouth as a long-term average. Indeed, they quantitatively agree well for the individual Siberian rivers (e.g., Zhang et al., 2012; Oshima et al., 2015). These variables are strongly affected by the *P* and associated atmospheric moisture transport over the individual regions (Figure 1). Processes of the moisture transport associated with the *P*-*E* show regional difference among the Siberian rivers (Oshima et al., 2015). The *P*-*E* over the Lena (Ob) is mainly supplied by a transient (stationary) moisture flux associated with cyclone activity (seasonal mean wind). Both processes affect the area over the Yenisei.

Regarding to the interannual variations, the moisture transport, *P*-*E*, *P*, and *R* also relate to each other, while those relationships have some seasonal time lag due to large area of the basin, snow accumulation in winter, negative or near zero *P*-*E* in summer and terrestrial processes as discussed in Oshima et al. (2015). More details about this are given in the last part of next section. Fukutomi et al. (2003) elucidated that the interannual variation in summer *P* over the Lena was negatively correlated with that over the Ob during the 1980s to mid-1990s. The summer *P*-*E* and autumn *R* of the two rivers were also negatively correlated in the same period. Furthermore, Fukutomi et al. (2003) indicated that the negative correlations were affected by an east–west seesaw pattern of atmospheric large-scale circulation and associated moisture transport over Siberia. When the *P* is large (small) over the Lena (Ob), cyclonic (anticyclonic) anomalies of atmospheric circulation emerge over the Lena (Ob) river basin. These anomalies result in a convergence and divergence of moisture flux over the basins and the coincident changes in *P* then produce the negative correlation of *R* between the two rivers. While the influence of cyclone activity on the interannual variations in *P*-*E* and *R* was discussed in their studies (Fukutomi et al., 2004, 2007, 2012), the cause of the negative correlations has not been fully explained, and it is not certain whether the negative correlation occurs in other periods.

The negative correlation noted above was apparent during the 1980s to mid-1990s. More recently, several drastic changes in the terrestrial water cycle have occurred around Yakutsk in eastern Siberia. Increases in *P* and soil moisture, and deepening of the active layer (Ohta et al., 2008, 2014; Iijima et al., 2010; Iwasaki et al., 2010) have been observed, particularly during 2005–2008, and the wet conditions have induced flooding (Fujiwara, 2011; Sakai et al., 2015) and forest degradation (Iwasaki et al., 2010; Iijima et al., 2014; Ohta et al., 2014). Moreover, effects of permafrost degradation on changing thermokarst lakes and landscapes have been reported in the last two decades (Fedorov et al., 2014). While these are local changes, the observed results suggest that some changes on a large spatial scale also occurred in this region in recent decades. Indeed, Iijima et al. (2016) showed that the increase in *P* and the wet conditions in eastern Siberia during the mid-2000s were affected by cyclone activity accompanied by changes in large-scale atmospheric circulation over Siberia. This suggests that the relationship between the Lena and Ob, which was negative correlation during the 1980s to mid-1990s, recently changed. However, the long-term variation and its effects on the water cycle in this region are still unclear.

Earth Syst. Dynam. Discuss., https://doi.org/10.5194/esd-2017-54
Manuscript under review for journal Earth Syst. Dynam.
Discussion started: 6 June 2017

To examine the long-term variation in *R* of the Lena and Ob Rivers, in addition to the observed *R* during the past seven decades, we analyzed reconstructed *R* based on tree rings during the past two centuries. We further examined an influencing factor on the long-term variation in *R* and *P*, and the associated atmospheric circulation using atmospheric reanalyses and simulations with an atmospheric general circulation model (AGCM) and atmosphere-ocean coupled models archived in the World Climate Research Programme's Coupled Model Intercomparison Project phase 3 (CMIP3).

2 Data and analysis methods

Monthly *R* observed near the river mouths of the Lena and Ob (i.e., Kusur and Salehard, Figure 1) from the Arctic-Rapid Integrated Monitoring System for the period of 1936–2009 (http://rims.unh.edu/), and the reconstructed annual *R* based on tree rings for the period of 1800–1990 (MacDonald et al., 2007, http://onlinelibrary.wiley.com/doi/10.1029/2006JG000333) were used. Because of limitations on the time period, in addition to the entire period, we analyzed subsets of 150-year periods for the reconstructed *R*. There is a 191-year record of reconstructed *R*, and we produced 5 subsets of 150-year records, with the start years delayed successively by one decade.

Monthly *P* from the Global Precipitation Climatology Center (GPCC, Schneider et al., 2013) was compared to the *R*. For simplicity, we defined the area of 50–70°N and 110–135°E as the Lena region, and the area of 50–70°N and 60–85°E as the Ob region. The area averaged *P* over these regions corresponded well with the averages over the individual river basins. The correlations were 0.89 for the Lena and 0.86 for the Ob. In analyses of atmospheric circulation, geopotential height at 500 hPa (*Z500*) from two atmospheric reanalyses, the Japanese 55-year Reanalysis (JRA-55, Kobayashi et al., 2015; Harada et al., 2016) and the National Oceanic and Atmospheric Administration-Cooperative Institute for Research in Environmental Sciences (NOAA/CIRES) Twentieth Century Reanalysis (20CR, Compo et al., 2011), was used. The time period of the *P* and *Z500* datasets was from 1901 to 2010, except for the JRA-55, which started from 1958.

There are long-term records of tree-ring-reconstructed *R*s over the past two centuries, whereas the meteorological data are limited to the 20th century. To examine the long-term variation and intrinsic atmospheric circulation associated with the *P*, a 300-year control simulation was performed with an AGCM developed by the Center for Climate System Research, University of Tokyo, and the National Institute for Environmental Studies (Numaguti et al., 1995, 1997). The setting of the control simulation was the same as in Ogata et al. (2013). The horizontal resolution was about 300 km and the vertical level was 20 layers (T42L20). It started from a state of rest with constant temperature, and was forced by the climatological seasonal cycle of sea surface temperature (SST), sea ice, and fixed greenhouse gases (GHG) as boundary conditions. We excluded the first 5 years of data from the 300-year simulation as the spin-up time. As in the reconstructed *R*, for the AGCM control simulation, we made 15 subsets of 150-year records, with the start years delayed successively by one decade.

In addition, control simulations under pre-industrial conditions (PICTL) and "the 20th century climate in coupled models" (20C3M) simulations in the CMIP3 multi-models conducted for the Fourth Assessment Report of the Intergovernmental Panel on Climate Change (IPCC AR4, Meehl et al., 2007) were compared to the AGCM control simulation. 23 CMIP3 models with all of the multi-ensemble members were used. While the time periods of the CMIP3 simulations were different

among the models, the 20C3M simulations were from 1850–1900 to 2000–2001. The PICTL simulations had time records from 81 to 1001 years. We analyzed the PICTL simulations that were longer than 150 years and made subsets of 150-year records with the start years delayed successively by five decades in each of the PICTL simulations.

Although the reconstructed *R* was an annual value, we analyzed seasonal mean values for the observed *R*, *P*, and *Z500*, because there is a seasonal time lag between *P* and *R* and the atmospheric circulation and *P* have large seasonality. The summer *P*-*E* may correspond to autumn *R* as in Tachibana et al. (2008), and the summer *P*-*E* and *P* are governed by atmospheric circulation in summer. In the similar method of Tachibana et al. (2008), we compared all possible combinations of *P*-*E* and *R* pairs and found that summer period from June to September and autumn period from August to October are best match for the Lena and Ob Rivers. The correlations during 1936–2009are 0.79 for the Lena and 0.64 for the Ob, both significant above the 99% significance level (Table 1). In addition, due to the large amount and large variability of water vapor in summer, it is expected that the interannual variations in summer *P* and corresponding autumn *R* dominate the annual values. While those were still indicated in the previous studies (Fukutomi et al., 2003; Zhang et al., 2012), we confirmed the contribution of seasonal values of *P* and *R* to annual values. The correlation between the summer *P*-*E* (autumn *R*) and its annual value is 0.91 (0.79) for the Lena, and that for the Ob is 0.64 (0.91). Therefore, we employed the summer *P* and *Z*500 during June to September and autumn *R* during August to October in the analysis.

3 Results

3.1 Long-term variation

3.1.1 Observed and reconstructed river discharges

Figure 2a shows the time-series of observed autumn *R* at the river mouths of the Lena (red solid line) and Ob (red dashed line) during the past seven decades (1936–2009), with 15-year running correlations between them (black line). Although the correlations were strong and negative during the 1980s to mid-1990s as in Fukutomi et al. (2003), those were positive during the 1950s to 1960s and became weak after the 1990s. As mentioned above, these autumn *Rs* correspond to the summer *Ps*. The time-series of the summer *P* over the Lena and Ob regions (Figure 2b) indicate a negative correlation around the 1910s, during the 1940s to mid-1950s, and after the 1980s. The correlations of *P* were near zero in the 1920s, and were weak and positive during the 1940s to 1950s. While there were some differences between the observed *R* and *P*, the *P* displayed a strong negative correlation in the 1980s, with no correlation in the 2000s. These results from the observations indicate that the relationship between the *R* and *P* of the Lena and Ob were different in each of the epochs.

Figure 2c shows a long-term time-series of tree-ring-reconstructed annual *R* of the Lena and Ob during the past two centuries (1800–1990). Similar to the observation, the correlations of reconstructed *R* were negative during the 1980s to mid-1990s and positive during the 1950s to 1960s, while there was some discrepancy between the observed *P* and reconstructed *R* in the early 20th century. The discrepancy may be due to errors both in the reconstruction and observation. In the 19th century, the correlations of reconstructed *R* were strong and negative in some epochs (1810s, 1850s, and 1890s) and

moderate or weak and positive in some other epochs (1880s and 1900s). These results also indicate that the relationship between the Lena and Ob differed in each epoch. However, it is noteworthy that negative correlations were frequently seen in the time series of reconstructed *R* (black line in Figure 2c). As shown by the red bar histogram in Figure 3a, many of the correlations for reconstructed *R* were negative. The correlations of observed *R* and *P* also tended to have negative values, although these results may not be as robust due to relatively short records (observed *R*: 74 years, *P*: 111 years). As a result, the medians of these correlations were negative and their skewnesses were positive (Table 2, Figure 3b). Therefore, the interannual variation in *R*s/*P*s of the Lena and Ob Rivers has tended to be out of phase during the past two centuries. This may suggest that the east–west seesaw pattern frequently emerges over Siberia.

3.1.2 Simulated precipitation

To determine the intrinsic atmospheric circulation associated with the variation in summer *P*, we examined the AGCM control simulation. As with the reconstructed *R*, the correlations between the simulated summer *P* over the Lena and Ob regions were largely negative (Table 2 and Figure 3). Compared to the reconstructed *R*, the distribution of simulated *P* was more negative than positive (Figure 3a) and the median and skewness from the simulated summer *P* (Table 2) tended to be more negative and positive, respectively (Figure 3b). These results indicate that atmospheric internal variability in summer leads to the out-of-phase summer *P*. The AGCM control simulation has no external forcing, and boundary conditions such as SST, sea ice, solar activity, and GHG are fixed. Consequently, the variation in simulated *P* and *Z500* in the control simulation can be interpreted as internal variability in the model.

The 20C3M and PICTL simulations in the CMIP3 coupled models provided more evidence for intrinsic atmospheric variability, including air–sea interactions. The medians and skewness of the correlations between the summer *P* over the Lena and Ob regions in the CMIP3 simulations are plotted in Figure 3b; they also tended to be negative and positive, respectively, but they were well scattered. This suggests that some models failed to reproduce the summer *P* variability and atmospheric circulation over Siberia. However, note that many simulation results were plotted around the reconstructed *R* and most results from the CMIP3 simulations were distributed toward the center compared to those from the AGCM control simulation (Figure 3b). These results imply some effects of air–sea interactions on the *P* variability over the Lena and Ob. This is discussed in the final section.

While there were weak and positive correlations of summer *P* in several periods (Figures 2 and 3a), we focused on the negative correlation and further examined summertime atmospheric circulation pattern associated with the *P* over Siberia.

3.2 Atmospheric circulation associated with the negative correlation of precipitations

To identify the summertime dominant atmospheric circulation patterns associated with summer *P* variability, we performed an empirical orthogonal function (EOF) analysis on summer *Z500* over the three great Siberian river basins (blue inset box in Figure 4). The spatial pattern of the first EOF mode (EOF1) was the cyclonic circulation anomaly centered in the vicinity of the coast in central Siberia (not shown). This pattern only enhances the eastward moisture transport over Siberia,

Earth Syst. Dynam. Discuss., https://doi.org/10.5194/esd-2017-54
Manuscript under review for journal Earth Syst. Dynam.
Discussion started: 6 June 2017

and the effect on moisture convergence/divergence over the Lena and Ob regions is small. The EOF2 indicated an east–west seesaw pattern similar to Fukutomi et al., (2003). While Figure 4 is based on the JRA-55, the result of 20CR showed a similar pattern to that of EOF2, for which the pattern correlation was 0.89. The seesaw pattern of EOF2 directly affects moisture convergence and divergence over the two river basins and results in changes in the *P* over the regions.

To confirm the effects of the east–west seesaw pattern on the *P*, we compared the difference in *Z500* over the western and eastern Siberia regions (west–east difference in *Z500*: $\Delta Z500_{WE}$) and the difference in *P* over the Lena and Ob regions (Lena–Ob difference in *P*: ΔP_{LO}). We defined the Lena and Ob regions for *P* (green inset boxes in Figure 4), which cover almost all of the basins, while the regions for the *Z500* were shifted 10° westward (purple inset boxes), which covered almost all of the negative and positive centers of action of EOF2. As described in the Introduction, when *Z500* anomalies are negative over the east and positive over the west as shown in Figure 4, *P* anomalies must be positive over the Lena region and negative over the Ob region. As expected, ΔP_{LO} was positively correlated with $\Delta Z500_{WE}$. The correlation coefficients were 0.72 for the JRA-55 and 0.60 for the 20CR, both significant above the 99% significance level (Figure 5).

Similar results (i.e., the east–west seesaw pattern of EOF2 and the positive correlation between the ΔP_{LO} and $\Delta Z500_{WE}$) were obtained in the AGCM control simulation and in the 20C3M and PICTL simulations from the CMIP3 coupled models, while some CMIP3 simulations failed to reproduce these features. The pattern correlation between the EOF2 patterns of the JRA-55 and AGCM was 0.83. The correlations for the 20C3M and PICTL simulations ranged from -0.62 to 0.94, but in 81% of the 20C3M and 76% of the PICTL simulations the correlations were greater than 0.7. Several CMIP3 models simulated the east–west pattern in the EOF3. The correlation between the ΔP_{LO} and $\Delta Z500_{WE}$ in the AGCM was 0.55 for the entire period of the 295-year record and 0.53–0.63 for the 15 subsets of 150-year records. The correlations between the ΔP_{LO} and $\Delta Z500_{WE}$ in 94% of the 20C3M and 90% of the PICTL simulations were greater than 0.7. Therefore, the results of the simulations of the AGCM and CMIP3 models were basically consistent with the reconstructed *R* and observations, and they support the linkage between the summertime east–west seesaw pattern over Siberia and the out-of-phase *P* over the Lena and Ob regions.

4 Summary and discussion

We examined the long-term variation in the *R*s and corresponding *P*s for the Lena in eastern Siberia and the Ob in western Siberia based on observations, tree ring reconstructions, and simulations with the AGCM and CMIP3 models. The observations during the past seven decades indicated that correlations between the observed *R*s of the Lena and Ob were negative during the 1980s to mid-1990s as in Fukutomi et al., (2003), but positive during the mid-1950s to 60s and became weak in recent decades (Figure 2a). This suggests that the relationship between the Lena and Ob *R*s was different in each of the epochs. However, the reconstructed *R*s indicated that the Lena and Ob tended to be negatively correlated, i.e., out of phase during the past two centuries (Figures 2c and 3). The observed *P*s over eastern and western Siberia also had negative correlations in the 20th century, which were affected by the east–west seesaw pattern of summertime atmospheric circulation over Siberia (Figure 4). Compared to the reconstructed *R* and observed *P*, the simulated *P*s in the AGCM control simulation

indicated more frequent negative correlations in association with the seesaw pattern (Figure 3). Because of the fixed boundary conditions, the control simulation demonstrated that the negative correlation and the seesaw pattern emerge as summertime atmospheric internal variability over Siberia. Although the results from the 20C3M and PICTL simulations vary among the models, they basically support the above features. As a consequence, the east–west seesaw pattern of atmospheric circulation frequently emerges as summertime atmospheric internal variability over Siberia and affects the negative correlation of the summer *P*s over eastern and western Siberia, resulting in the out-of-phase autumn *R*s of the Lena and Ob Rivers. Therefore, the summertime atmospheric internal variability of the seesaw pattern over Siberia is a key factor influencing the water cycles in this region.

The results in simulations give us several more implications for the *P* variability and the east–west seesaw pattern over Siberia. Compared to the AGCM control simulation, the CMIP3 simulations mostly plotted around the reconstructed *R* (Figure 3b), suggesting that the air–sea interaction acts as a dumping of the seesaw pattern and the negative correlation of *P*. Moreover, while the negative correlation of *P* was related to atmospheric internal variation, the positive correlation may have been affected by an external forcing such as an SST or sea ice anomaly. Indeed, Sun et al. (2015) reported the remote influence of Atlantic multidecadal variation, which is an oscillation of North Atlantic SST between basin-wide uniform warm and cold conditions, on the variation in summertime *P* over Siberia on decadal or multidecadal timescales. Iwao and Takahashi (2006, 2008) indicated that the effects of quasi-stationary Rossby waves originated from blocking anticyclones in the North Atlantic–European sector on the precipitation seesaw pattern between northeast Asia and eastern Siberia. Iijima et al. (2016) indicated the impact of enhanced storm activity on an increase in *P* and permafrost degradation in eastern Siberia during the mid-2000s and they discussed the relationship with the Arctic dipole anomaly associated with the sea ice reduction. Fujinami et al. (2016) and Hiyama et al. (2016) also showed the similar result for the *P* over eastern Siberia. While they studied somewhat different time scales and different regions, the variation in *P* over the Lena and Ob must be affected by a combination of these processes including internal variability. In addition, it seems that the differences between the 20C3M and PICTL simulations are not large (Figure 3b), and there should be no significant influence of changes in GHG on the long-term variation in *P* in Siberia, while *P* in future projections will increase under global warming (IPCC AR4 WG1 2007, AR5 WG1 2013).

Acknowledgments

This work was supported partly by the JSPS KAKENHI Grant Number 24241009 and 26340018, the GRENE Arctic Climate Change Research Project, the Arctic Challenge for Sustainability (ArCS) Project and the Joint Research Program of the Japan Arctic Research Network Center.

References

Aagaard, K. and Carmack, E. C.: The role of sea ice and other fresh water in the Arctic circulation, J. Geophys. Res.: Oceans, 94, 14485–14498, doi:10.1029/JC094iC10p14485, 1989.

Aagaard, K. and Carmack, E. C.: The Arctic Ocean and Climate: A Perspective, in The Polar Oceans and Their Role in Shaping the Global Environment, Johannessen, O. M., Muench R. D., and Overland, J. E. eds., American Geophysical Union, 5–20, doi:10.1029/GM085p0005, 1994.

Berezovskaya, S.: Compatibility analysis of precipitation and runoff trends over the large Siberian watersheds, Geophys. Res. Lett., 31, doi:10.1029/2004gl021277, 2004.

Compo, G. P., Whitaker, J. S., Sardeshmukh, P. D., Matsui, N., Allan, R. J., Yin, X., Gleason, B. E., Vose, R. S., Rutledge, G., Bessemoulin, P., Brönnimann, S., Brunet, M., Crouthamel, R. I., Grant, A. N., Groisman, P. Y., Jones, P. D., Kruk, M. C., Kruger, A. C., Marshall, G. J., Maugeri, M., Mok, H. Y., Nordli, Ø., Ross, T. F., Trigo, R. M., Wang, X. L., Woodruff, S. D., and Worley, S. J.: The Twentieth Century Reanalysis Project, Q. J. Roy. Meteor. Soc., 137, 1–28, doi:10.1002/qj.776, 2011.

Fedorov, A. N., Gavriliev, P. P., Konstantinov, P. Y., Hiyama, T., Iijima, Y., and Iwahana, G.: Estimating the water balance of a thermokarst lake in the middle of the Lena River basin, eastern Siberia, Ecohydrology, 7, 188–196, doi:10.1002/eco.1378, 2014.

Fujinami, H., Yasunari, T., and Watanabe T.: Trend and inter-annual variation in summer precipitation in eastern Siberia in re-cent decades. Int. J. Climatol., 36, 355–368, doi:10.1002/joc.4352, 2016.

Fujiwara, J.: Climate change and migration policy in the Republic of Sakha, FY2010 FR22 Research Project Report “Global warming and the Human-Nature Dimension in Siberia: Social adaptation to the changes of the terrestrial ecosystem, with an emphasis on water environments (RIHN Project C-07) , Research Institute for Humanity and Nature, Hiyama, T. eds., 192–196, 2011. (in Japanese).

Fukutomi, Y., Igarashi, H., Masuda, K., and Yasunari, T.: Interannual Variability of Summer Water Balance Components in Three Major River Basins of Northern Eurasia, J. Hydrometeorol., 4, 283–296, doi:10.1175/1525-7541(2003)4<283:IVOSWB>2.0.CO;2, 2003.

Fukutomi, Y., Masuda, K., and Yasunari, T.: Role of storm track activity in the interannual seesaw of summer precipitation over northern Eurasia, J. Geophys. Res.: Atmospheres, 109, D02109, doi:10.1029/2003JD003912, 2004.

Fukutomi, Y., Masuda, K., and Yasunari, T.: Cyclone activity associated with the interannual seesaw oscillation of summer

precipitation over northern Eurasia, Global and Planetary Change, 56, 387–398, doi:10.1016/j.gloplacha.2006.07.026, 2007.

Fukutomi, Y., Masuda, K., and Yasunari, T.: Spatiotemporal structures of the intraseasonal oscillations of precipitation over northern Eurasia during summer, Int. J. Climatol., 32, 710–726, doi:10.1002/joc.2293, 2012.

Harada, Y., Kamahori, H., Kobayashi, C., Endo, H., Kobayashi, S., Ota, Y., Onoda, H., Onogi, K., Miyaoka, K., and Takahashi, K.: The JRA–55 Reanalysis: Representation of Atmospheric Circulation and Climate Variability, J. Meteor. Soc. Japan, 94, 269–302, doi:10.2151/jmsj.2016-015, 2016.

Hiyama, T., Fujinami, H., Kanamori, H., Ishige, T., and Oshima, K.: Interdecadal modulation of the interannual variability in precipitation and atmospheric circulation pattern over northern Eurasia, Env. Res. Lett., 11 ,065001, doi:10.1088/1748-9326/11/6/065001, 2016.

Iijima, Y., Fedorov, A. N., Park, H., Suzuki, K., Yabuki, H., Maximov, T. C., and Ohata, T.: Abrupt increases in soil temperatures following increased precipitation in a permafrost region, central Lena River basin, Russia, Permafrost Periglac., 21, 30–41, doi:10.1002/ppp.662, 2010.

Iijima, Y., Nakamura, T., Park, H., Tachibana, Y., and Fedorov, A. N.: Enhancement of Arctic storm activity in relation to permafrost degradation in eastern Siberia, Int. J. Climatol., 36, 4265–4275, doi:10.1002/joc.4629, 2016.

Iijima, Y., Ohta, T., Kotani, A., Fedorov, A. N., Kodama, Y., and Maximov, T. C.: Sap flow changes in relation to permafrost degradation under increasing precipitation in an eastern Siberian larch forest, Ecohydrology, 7, 177–187, doi:10.1002/eco.1366, 2014.

IPCC, Climate Change 2007: The Physical Science Basis. Contribution of Working Group I to the Fourth Assessment Report (AR4) of the Intergovernmental Panel on Climate Change, Solomon, S., Qin, D., Manning, M., Chen, Z., Marquis, M., Averyt, K. B., Tignor, M., and Miller H. L., eds., Cambridge University Press, 996 pp, 2007.

IPCC, Climate Change 2013: The Physical Science Basis. Contribution of Working Group I to the Fifth Assessment Report (AR5) of the Intergovernmental Panel on Climate Change, Stocker, T.F., Qin, D., Plattner, G.-K., Tignor, M. , Allen, S. K., Boschung, J., Nauels, A., Xia, Y., Bex, V., and Midgley, P.M. eds., Cambridge University Press, 1535 pp, 2013.

Iwao, K. and Takahashi, M.: Interannual change in summertime precipitation over northeast Asia, Geophys. Res. Lett., 33, doi:10.1029/2006GL027119, 2006.

Iwao, K. and Takahashi, M.: A Precipitation Seesaw Mode between Northeast Asia and Siberia in Summer Caused by Rossby Waves over the Eurasian Continent, J. Climate, 21, 2401–2419, doi:10.1175/2007JCLI1949.1, 2008.

Iwasaki, H., Saito, H., Kuwao, K., Maximov, T. C., and Hasegawa, S.: Forest decline caused by high soil water conditions in a permafrost region, Hydrol. Earth Syst. Sci., 14, 301–307, doi:10.5194/hess-14-301-2010, 2010.

Kobayashi, S., Ota, Y., Harada, Y., Ebita, A., Moriya, M., Onoda, H., Onogi, K., Kamahori, H., Kobayashi, C., Endo, H., Miyaoka, K., and Takahashi, K.: The JRA–55 Reanalysis: General Specifications and Basic Characteristics, J. Meteor. Soc. Japan, 93, 5–48, doi:10.2151/jmsj.2015-001, 2015.

MacDonald, G. M., Kremenetski, K. V., Smith, L. C., and Hidalgo, H. G.: Recent Eurasian river discharge to the Arctic

Ocean in the context of longer–term dendrohydrological records, J. Geophys. Res., 112, doi:10.1029/2006jg000333, 2007.

McClelland, J. W., Déry, S. J., Peterson, B. J., Holmes, R. M., and Wood, E. F.: A pan–arctic evaluation of changes in river discharge during the latter half of the 20th century, Geophys. Res. Lett., 33, doi:10.1029/2006gl025753, 2006.

McClelland, J. W., Holmes, R. M., Peterson, B. J., and Stieglitz, M.: Increasing river discharge in the Eurasian Arctic: Consideration of dams, permafrost thaw, and fires as potential agents of change, J. Geophys. Res.: Atmospheres, 109, D18102, doi:10.1029/2004JD004583, 2004.

Meehl, G. A., Covey, C., Taylor, K. E., Delworth, T., Stouffer, R. J., Latif, M., McAvaney, B., and Mitchell, J. F. B.: THE WCRP CMIP3 Multimodel Dataset: A New Era in Climate Change Research, Bull. Am. Meteorol. Soc., 88, 1383–1394, doi:10.1175/bams-88-9-1383, 2007.

Numaguti, A., Takahashi, M., Nagajima, T., and Sumi, A.: Development of an atmospheric general circulation model. In Reports of a New Program for Center Basic Research Studies, Studies of Global Environment Change with Special Reference to Asia and Pacific Regions, Rep. I-3, 1–27, CCSR. Tokyo, 1995.

Numaguti, A., Sugata, S., Takahashi, M., Nakajima, T., and Sumi, A.: Study on the climate system and mass transport by a climate model, CGER's supercomputer monograph report, 3, 91 pp, 1997.

Ogata, K., Tachibana, Y., Udagawa, Y., Oshima K., and Yoshida, K.: Influence of sea ice anomaly in the Pacific sector of the Southern Ocean upon atmospheric circulation using an AGCM, Umi to Sora, 89(1), 19–23, 2013. (in Japanese).

Ohta, T., Kotani, A., Iijima, Y., Maximov, T. C., Ito, S., Hanamura, M., Kononov, A. V., and Maximov, A. P.: Effects of waterlogging on water and carbon dioxide fluxes and environmental variables in a Siberian larch forest, 1998–2011, Agric. For. Meteorol., 188, 64–75, doi:10.1016/j.agrformet.2013.12.012, 2014.

Ohta, T., Maximov, T. C., Dolman, A. J., Nakai, T., van der Molen, M. K., Kononov, A. V., Maximov, A. P., Hiyama, T., Iijima, Y., Moors, E. J., Tanaka, H., Toba, T., and Yabuki, H.: Interannual variation of water balance and summer evapotranspiration in an eastern Siberian larch forest over a 7–year period (1998–2006), Agric. For. Meteorol., 148, 1941–1953, doi:10.1016/j.agrformet.2008.04.012, 2008.

Oshima, K., Tachibana, Y., and Hiyama, T.: Climate and year–to–year variability of atmospheric and terrestrial water cycles in the three great Siberian rivers, J. Geophys. Res.: Atmos., 120, doi:10.1002/2014JD022489, 2015.

Rawlins, M. A., Willmott, C. J., Shiklomanov, A., Linder, E., Frolking, S., Lammers, R. B., and Vörösmarty, C. J.: Evaluation of trends in derived snowfall and rainfall across Eurasia and linkages with discharge to the Arctic Ocean, Geophys. Res. Lett., 33, doi:10.1029/2005GL025231, 2006.

Sakai, T., Hatta, S., Okumura, M., Hiyama, T., Yamaguchi, Y., and Inoue, G.: Use of Landsat TM/ETM+ to monitor the spatial and temporal extent of spring breakup floods in the Lena River, Siberia, Int. J. Remote Sens., 36, 719–733, doi:10.1080/01431161.2014.995271, 2015.

Schneider, U., Becker, A., Finger, P., Meyer–Christoffer, A., Ziese, M., and Rudolf, B.: GPCC's new land surface precipitation climatology based on quality–controlled in situ data and its role in quantifying the global water cycle, Theor.

Appl. Climatol., 115, 15–40, doi:10.1007/s00704-013-0860-x, 2013.

Serreze, M. C., Bromwich, D. H., Clark, M. P., Etringer, A. J., Zhang, T., and Lammers, R.: Large–scale hydro–climatology of the terrestrial Arctic drainage system, J. Geophys. Res., 108, doi:10.1029/2001jd000919, 2003.

Shiklomanov, A. I. and Lammers, R. B.: Record Russian river discharge in 2007 and the limits of analysis, Environ. Res. Lett., 4, 045015, doi:10.1088/1748-9326/4/4/045015, 2009.

Sun, C., Li, J., and Zhao, S.: Remote influence of Atlantic multidecadal variability on Siberian warm season precipitation, Sci. Rep., 5, 16853, doi:10.1038/srep16853, 2015.

Tachibana, Y., Oshima, K., and Ogi, M.: Seasonal and interannual variations of Amur River discharge and their relationships to large-scale atmospheric patterns and moisture fluxes, J. Geophys. Res., 113, D16102, doi:10.1029/2007JD009555, 2008.

Ye, H., Ladochy, S., Yang, D., Zhang, T., Zhang, X., and Ellison, M.: The Impact of Climatic Conditions on Seasonal River Discharges in Siberia, J. Hydrometeorol., 5, 286–295, doi:10.1175/1525-7541(2004)005<0286:TIOCCO>2.0.CO;2, 2004.

Zhang, X., He, J., Zhang, J., Polyakov, I., Gerdes, R., Inoue, J., and Wu, P.: Enhanced poleward moisture transport and amplified northern high–latitude wetting trend, Nature Clim. Change, 3, 47–51, doi:10.1038/nclimate1631, 2012.

Earth Syst. Dynam. Discuss., https://doi.org/10.5194/esd-2017-54
Manuscript under review for journal Earth Syst. Dynam.
Discussion started: 6 June 2017

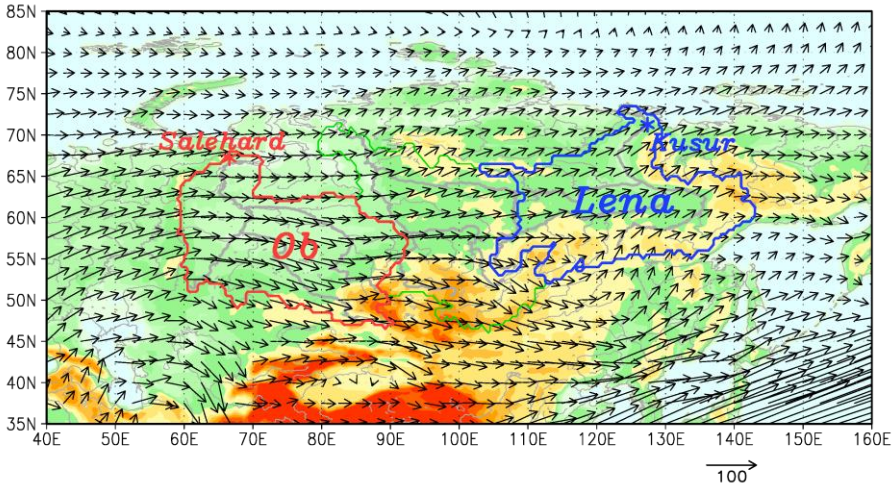

Figure 1: Map of study area of Siberia. The colored solid contours show the boundaries of each river basin (Lena: blue and Ob: red). The asterisks denote the locations of Kusur and Salehard, which are the observation stations nearest the river mouths. The vectors show climatological vertically integrated moisture flux (kg/m/s) in summer (June to September) averaged from 1981 to 2010 based on the JRA-55. The color and thick gray lines denote elevation and major flow paths, respectively.

Earth Syst. Dynam. Discuss., https://doi.org/10.5194/esd-2017-54
Manuscript under review for journal Earth Syst. Dynam.
Discussion started: 6 June 2017

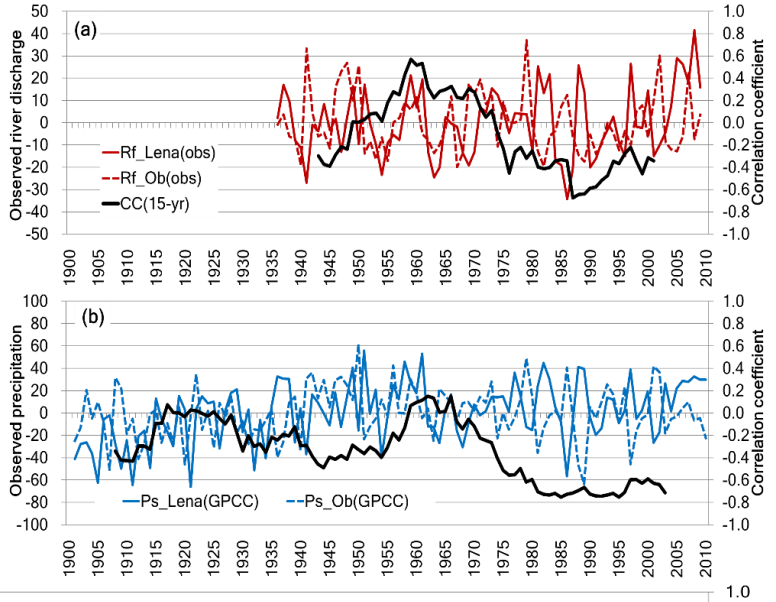

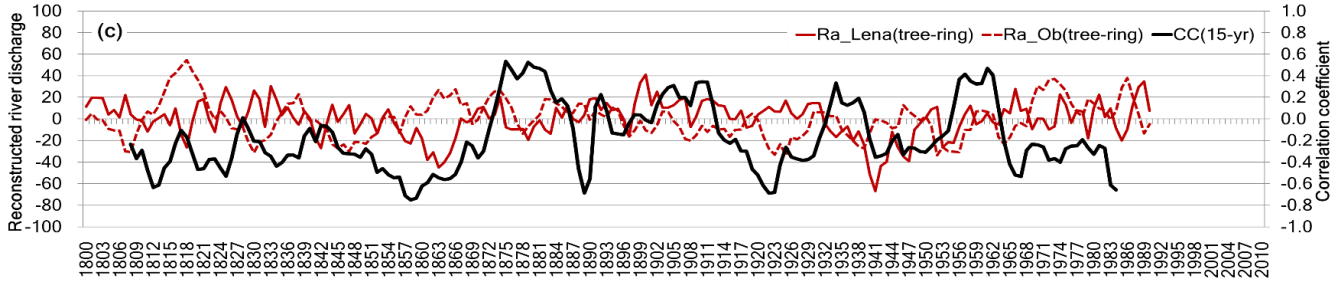

Figure 2: Time series of (a) observed autumn *R* during 1936–2009, (b) observed summer *P* during 1901–2010, and (c) tree-ring-reconstructed annual *R* during 1800–1990 of the Lena and Ob Rivers. Red (Blue) solid and dashed lines denote the *R*s (*P*s) of the Lena and Ob, respectively. Black thick lines denote 15-year running correlations between the Lena and Ob *R*s/*P*s. The significant levels at 90%, 95% and 98% for the 15-year correlation are 0.44, 0.51 and 0.59. Note that the axes of the *R* and *P* are shown on the left side of the panel and the axes of the correlations are shown on the right side.

Earth Syst. Dynam. Discuss., https://doi.org/10.5194/esd-2017-54
Manuscript under review for journal Earth Syst. Dynam.
Discussion started: 6 June 2017

Earth System Dynamics
Discussions
Open Access
EGU

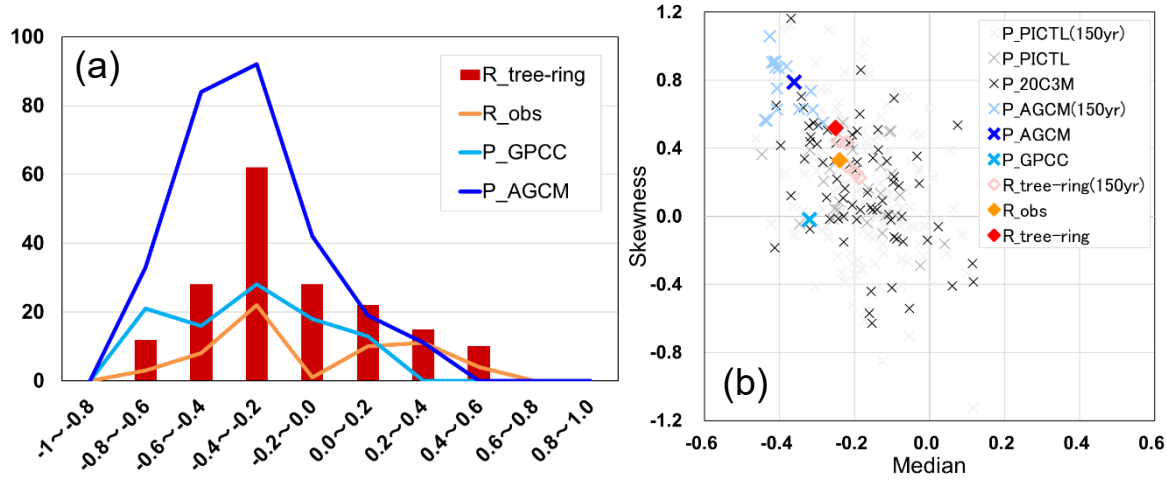

Figure 3: (a) Histogram of 15-year running correlations from the tree-ring-reconstructed annual *R* (red bars), observed autumn *R* (orange line), observed summer *P* (light blue line), and AGCM simulated summer *P* (blue line). (b) Scatter diagram between median and skewness of each of the 15-year correlations. Simulated *P* in the CMIP3 models' simulations (20C3M and PICTL), and subsets of 150-year record for the reconstructed *R* (5 samples), AGCM simulated *P* (15 samples), and PICTL simulated *P* (over 100 samples) are also plotted.

Earth Syst. Dynam. Discuss., https://doi.org/10.5194/esd-2017-54
Manuscript under review for journal Earth Syst. Dynam.
Discussion started: 6 June 2017

Earth System Dynamics
Discussions
Open Access
EGU

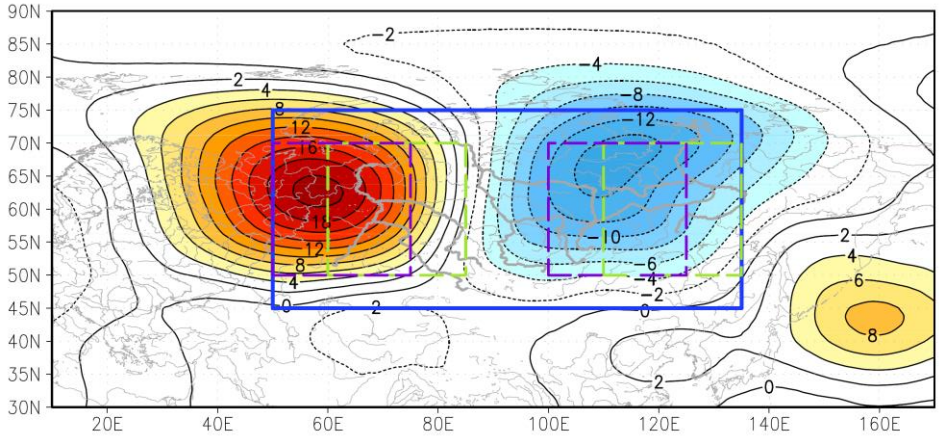

Figure 4: Spatial pattern of EOF2 (19.9% of explained variance) for the summertime *Z500* over Siberia region (blue line inset box: 45–75°N, 50–135°E, covering the three great Siberian rivers). Green (purple) dashed inset boxes cover almost all areas of the Lena and Ob river basins (western and eastern centers of action of EOF2). The EOF analysis is based on JRA-55.

Earth Syst. Dynam. Discuss., https://doi.org/10.5194/esd-2017-54
Manuscript under review for journal Earth Syst. Dynam.
Discussion started: 6 June 2017

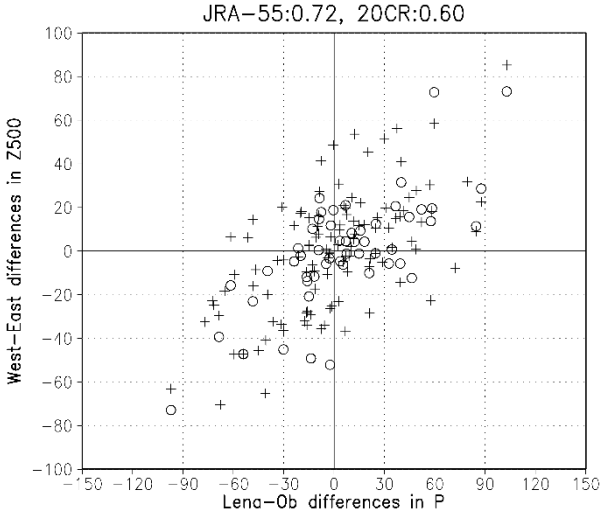

Figure 5: Scatter plot of the summer *P* differences between the Lena and Ob regions (ΔP_{LO}) and the summer *Z500* differences between the western and eastern Siberia regions ($\Delta Z500_{WE}$). The areas of ΔP_{LO} ($\Delta Z500_{WE}$) are defined as green (purple) dashed inset boxes in Figure 4. The $\Delta Z500_{WE}$ based on JRA-55 and 20CR are plotted as marked with circles and crosses. Correlation coefficients between ΔP_{LO} and $\Delta Z500_{WE}$ are shown in the upper side of the scatter plot.

Earth Syst. Dynam. Discuss., https://doi.org/10.5194/esd-2017-54
Manuscript under review for journal Earth Syst. Dynam.
Discussion started: 6 June 2017

Earth System Dynamics Discussions
Open Access
EGU

Table 1: Correlation coefficients among the summer *P*, annual *P*, autumn *R*, and annual *R* for (a) the Lena and (b) Ob Rivers during 1936–2009. Summer (autumn) averaging period is from June to September (from August to October). The *P* and *R* are based on the Arctic-RIMS and GPCC. All values are above the 99% significance level. Bold values are specifically described in the text.

Lena	Summer *P*	Annual *P*	Autumn *R*	Annual *R*
Summer *P*	1.00	**0.91**	**0.79**	0.66
Annual *P*		1.00	0.72	0.73
Autumn *R*			1.00	**0.79**
Annual *R*				1.00
Ob	Summer *P*	Annual *P*	Autumn *R*	Annual *R*
Summer *P*	1.00	**0.64**	**0.63**	0.57
Annual *P*		1.00	0.64	0.57
Autumn *R*			1.00	**0.91**
Annual *R*				1.00

Earth Syst. Dynam. Discuss., https://doi.org/10.5194/esd-2017-54
Manuscript under review for journal Earth Syst. Dynam.
Discussion started: 6 June 2017

Earth System Dynamics Discussions Open Access EGU

Table 2: Median and skewness of the 15-year running correlations for the tree-ring-reconstructed annual *R* (Figure 2c), observed autumn *R* (Figure 2a), observed summer *P* (Figure 2b), and simulated summer *P*. The observed *P* and simulated *P* are based on the GPCC and AGCM. A histogram and scatter diagram for these values are shown in Figure 3a and 3b. Values in brackets are the results from 5 (15) subsets of 150-year records for the reconstructed *R* (simulated *P*).

	Median	Skewness
***R*_tree-ring**	**-0.25** (-0.24 to -0.19)	**0.52** (0.23 to 0.44)
*R*_obs.	-0.24	0.33
*P*_GPCC	-0.32	-0.02
***P*_AGCM**	**-0.36** (-0.44 to -0.28)	**0.79** (0.55 to 1.06)